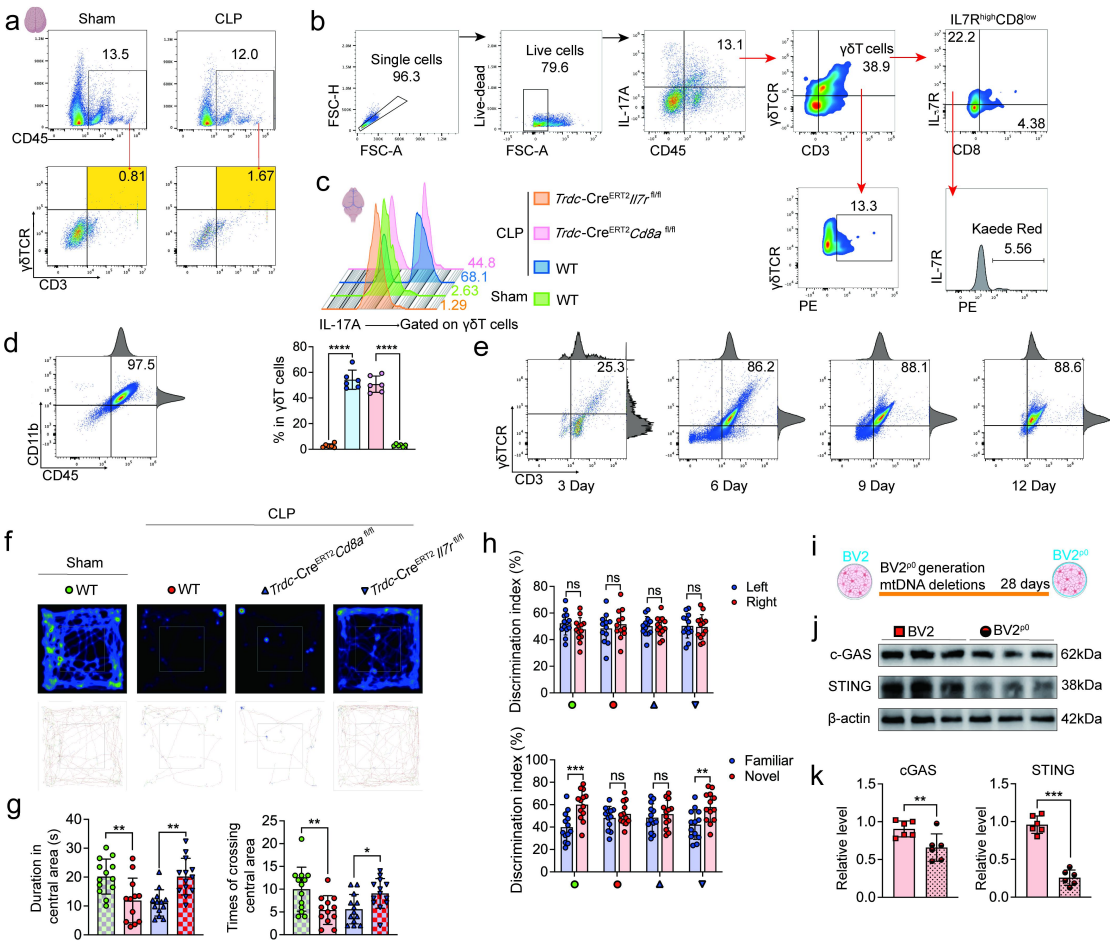

Extended Data Fig. 1. γδ T17 cells damage microglial mitochondria and induced SAE.

a Representative flow cytometry (FCM) plots showing CD45$^+$ γδ T cells (CD45$^+$ CD3$^+$ γδ TCR$^+$) in the brain of sham-operated and CLP-treated mice. **b** FCM gating strategy of Kaede red γδ T17 subgroups. **c** Representative FCM image showing IL-17A$^+$ γδ T cells (CD45$^+$ CD3$^+$ γδ TCR$^+$ IL-17A$^+$) in the meninges. Graph displaying the percentage of IL-17A$^+$ cells among γδ T cells in meninges (n = 6). **d** FCM analysis to assess the purity of primary microglial cells. **e** FCM analysis to assess the purity of primary γδ T cells. Representative images (**f**) and statistical analysis (**g**) of open field tests (n = 12–13). **h** Statistical analysis of novel object recognition tests (n = 12–13). **i** Treatment schedule. BV2 cells treated with ethidium bromide for 28 days to deplete

mitochondria, generating BV2$^{\rho 0}$ cells. Western blot (**j**) and quantification (**k**) of cGAS and STING in BV2 and BV2$^{\rho 0}$ cells treated with IL-17A and LPS (n = 6). Data are shown as mean ± SD. $^{*}P < 0.05$, $^{**}P < 0.01$, $^{***}P < 0.001$. ns, not significant. *P* values were calculated using one-way ANOVA followed by Šídák's multiple comparisons test (c, g), two-way ANOVA followed by Šídák's multiple comparisons test (h) and two-sided Student's unpaired t-tests (k).

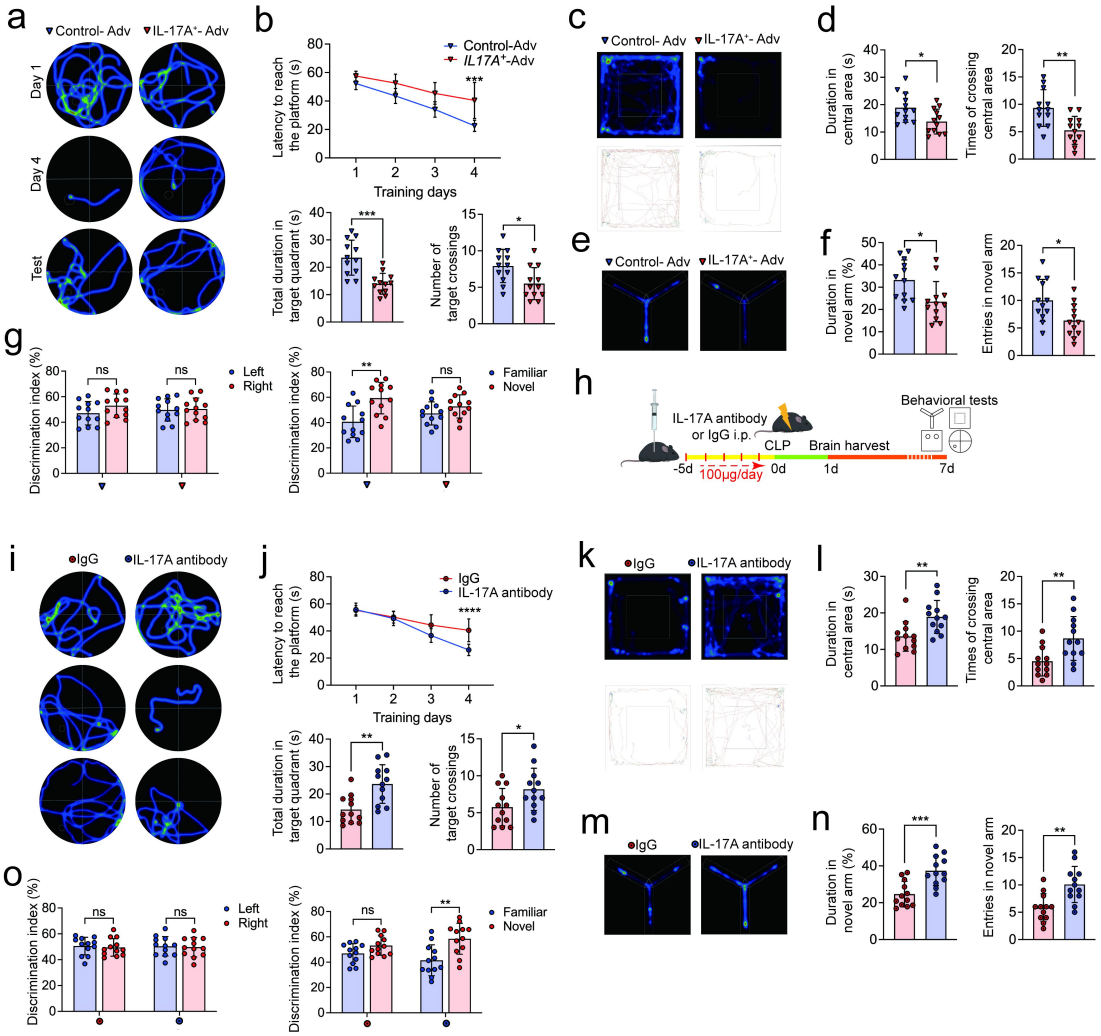

Extended Data Fig. 2. IL-17A exacerbates SAE.

Representative images (**a**) and statistical analysis (**b**) of Morris water maze (n = 12). Representative images (**c**) and statistical analysis (**d**) of open field tests (n = 12). Representative images (**e**) and statistical analysis (**f**) of Y-maze tests (n = 12). **g** Statistical analysis of novel object recognition tests (n = 12). **h** Treatment schedule. IL-17A neutralizing antibody or IgG (100 μg/day) was administered via intraperitoneal injection for 5 days, with four doses given prior to the cecum ligation and puncture (CLP) challenge and one dose immediately after. Brain tissues were collected 1 day post-CLP, and behavioral testing was conducted 7 days post-CLP. Representative images (**i**) and statistical analysis (**j**) of the Morris water maze (n = 12).

Representative images (**k**) and statistical analysis (**l**) of open field tests (n = 12). Representative images (**m**) and statistical analysis (**n**) of Y-maze tests (n = 12). **o** Statistical analysis of novel object recognition tests (n = 12). Data are shown as mean ± SD. $^{*}P < 0.05$, $^{**}P < 0.01$, $^{***}P < 0.001$. ns, not significant. *P* values were calculated using two-sided Student's unpaired t-tests (b, d, f, j, l, n) and multiple unpaired t-tests (g, o).

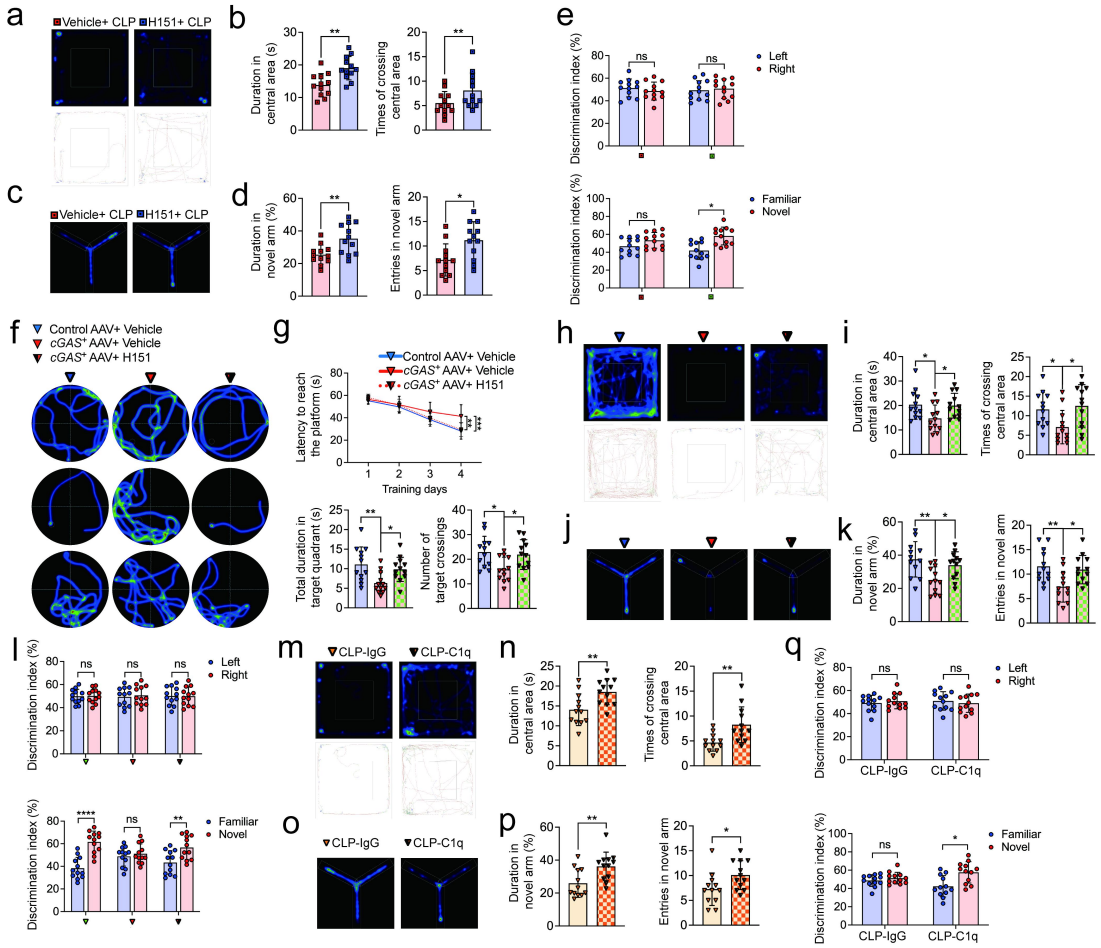

Extended Data Fig. 3. Activation of the cGAS-STING-C1q pathway exacerbates cognitive dysfunction.

Representative images (**a**) and statistical analysis (**b**) of open field tests (n = 12). Representative images (**c**) and statistical analysis (**d**) of Y-maze tests (n = 12). **e** Statistical analysis of novel object recognition tests (n = 12). Representative images (**f**) and statistical analysis (**g**) of the Morris water maze (n = 12). Representative images (**h**) and statistical analysis (**i**) of open field tests (n = 12). Representative images (**j**) and statistical analysis (**k**) of Y-maze tests (n = 12). **l** Statistical analysis of novel object recognition tests (n = 12). Representative images (**m**) and statistical analysis (**n**) of open field tests (n = 12). Representative images (**o**) and statistical analysis (**p**) of Y-maze tests (n = 12). **q** Statistical analysis of novel object recognition tests (n = 12).

Data are shown as mean ± SD. $^{*}P < 0.05$, $^{**}P < 0.01$, $^{****}P < 0.0001$. ns, not significant. *P* values were calculated using two-sided Student's unpaired t-tests (b, d, n, p), multiple unpaired t-tests (e, q), one-way ANOVA followed by Šídák's multiple comparisons test (g, i, k) and two-way ANOVA followed by Šídák's multiple comparisons test (l).

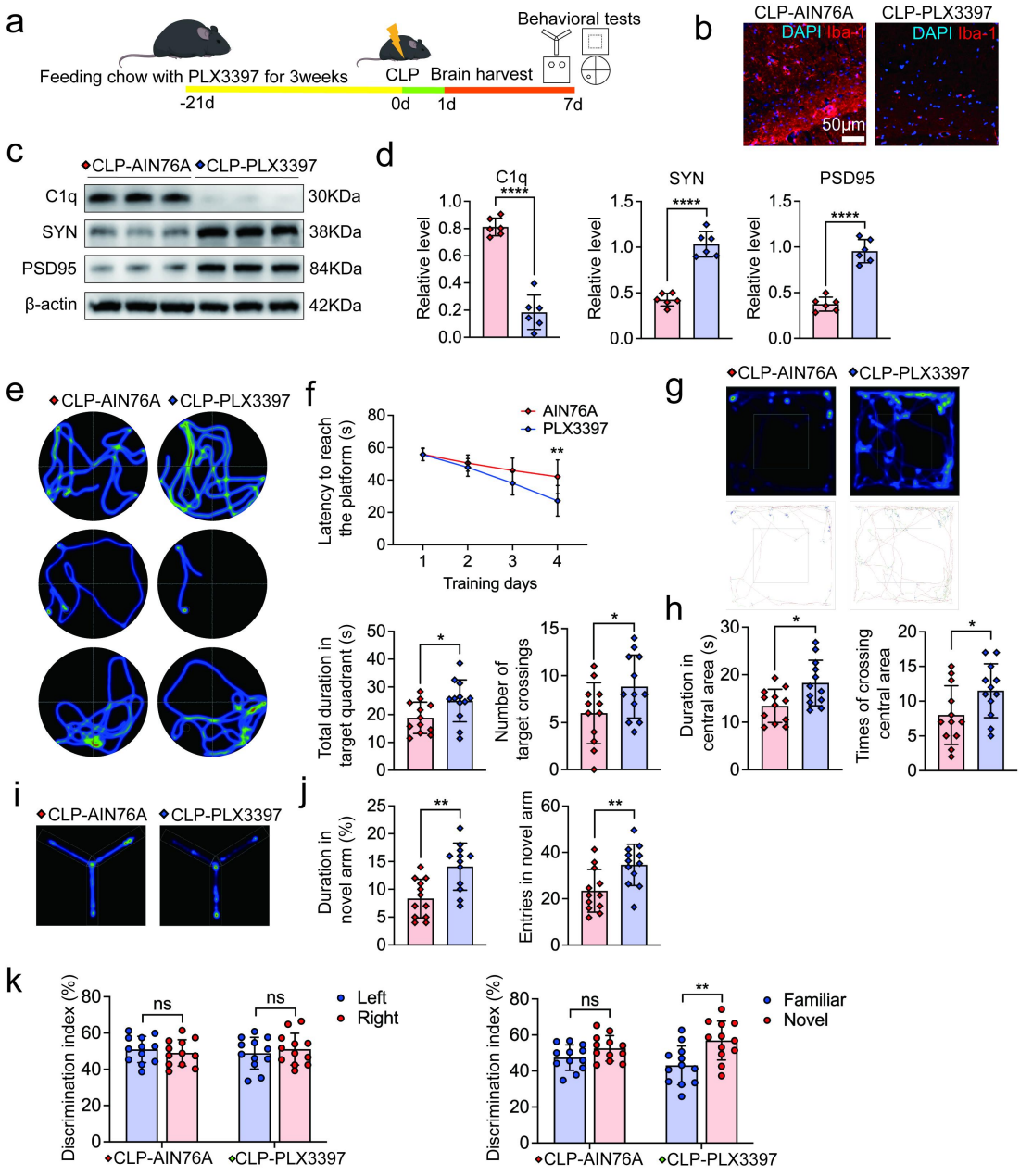

Extended Data Fig. 4. Microglia depletion ameliorates SAE.

a Treatment schedule. Mice were fed PLX3397 or AIN76A chow for 3 weeks prior to cecum ligation and puncture (CLP). Brain tissues were collected 1 day post-CLP, and behavioral testing was conducted 7 days post-CLP. **b** Representative immunofluorescence images showing microglia depletion in mice treated with PLX3397. Scale bar, 50 μm. Western blot (**c**) and quantification (**d**) of C1q, PSD95

and SYN in hippocampal synaptic proteins of mice fed with PLX3397 and AIN76A (n = 6). Representative images (**e**) and statistical analysis (**f**) of the Morris water maze (n = 12). Representative images (**g**) and statistical analysis (**h**) of open field tests (n = 12). Representative images (**i**) and statistical analysis (**j**) of Y-maze tests (n = 12). **k** Statistical analysis of novel object recognition tests (n = 12). Data are shown as mean ± SD. $^{*}P < 0.05$, $^{**}P < 0.01$, $^{****}P < 0.0001$. ns, not significant. *P* values were calculated using two-sided Student's unpaired t-tests (d, f, h, j) and multiple unpaired t-tests (k).

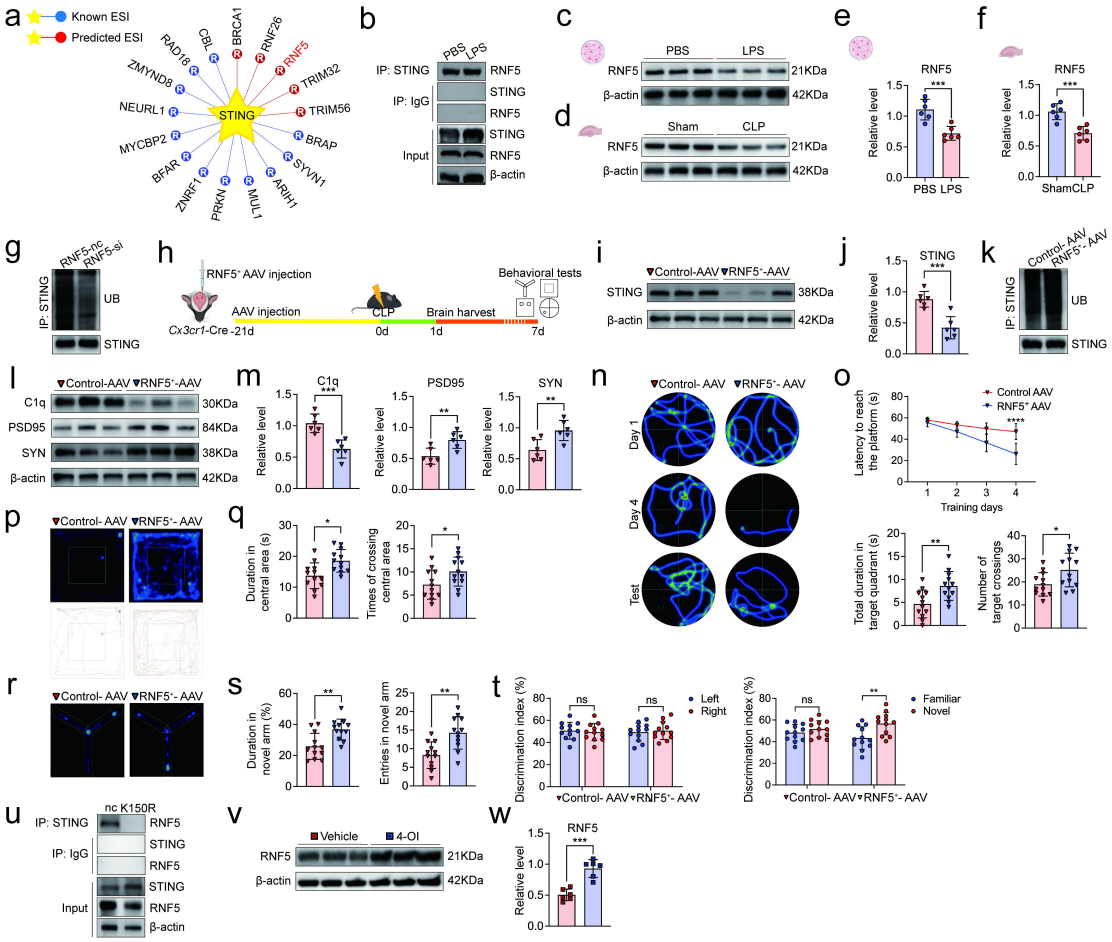

Extended Data Fig. 5. RNF5 enhances STING ubiquitination to mitigate SAE.

a Predicted E3 ubiquitin ligases for STING from the Ubibrowse database. **b** Co-immunoprecipitation and western blot analysis of the interaction between STING and RNF5 in BV2 cells. Western blot and quantification of RNF in primary microglia (**c, e**) and hippocampus (**d, f**) of mice (n = 6). **g** Western blot showing STING ubiquitination levels in primary microglia. **h** Treatment schedule. Hippocampal stereotactic injection of RNF5^{+} adeno-associated virus (AAV); cecum ligation and puncture (CLP) performed 21 days later. Brain tissues collected 1 day post-CLP, behavioral testing conducted 7 days post-CLP. Western blot (**i**) and quantification (**j**) of STING in the hippocampus of mice treated with control and RNF5^{+} AAV (n = 6). **k** Western blot image of STING ubiquitination levels in the hippocampus of mice

treated with control and RNF5^{+} AAV. Western blot (**l**) and quantification (**m**) of C1q, PSD95 and SYN in hippocampal synaptic proteins of mice treated with control and RNF5^{+} AAV (n = 6). Representative images (**n**) and statistical analysis (**o**) of the Morris water maze (n = 12). Representative images (**p**) and statistical analysis (**q**) of open field tests (n = 12). Representative images (**r**) and statistical analysis (**s**) of Y-maze tests (n = 12). **t** Statistical analysis of novel object recognition tests (n = 12). **u** Co-immunoprecipitation and western blot analysis of the interaction between STING and RNF5 in BV2 cells. Western blot (**v**) and quantification (**w**) of RNF in hippocampus of septic mice received 4-OI or vehicle (n = 6). Data are shown as mean ± SD. $^{*}P < 0.05$, $^{**}P < 0.01$, $^{***}P < 0.001$, $^{****}P < 0.0001$. ns, not significant. *P* values were calculated using two-sided Student's unpaired t-tests (e, f, j, m, q, o, s, w) and multiple unpaired t-tests (t).

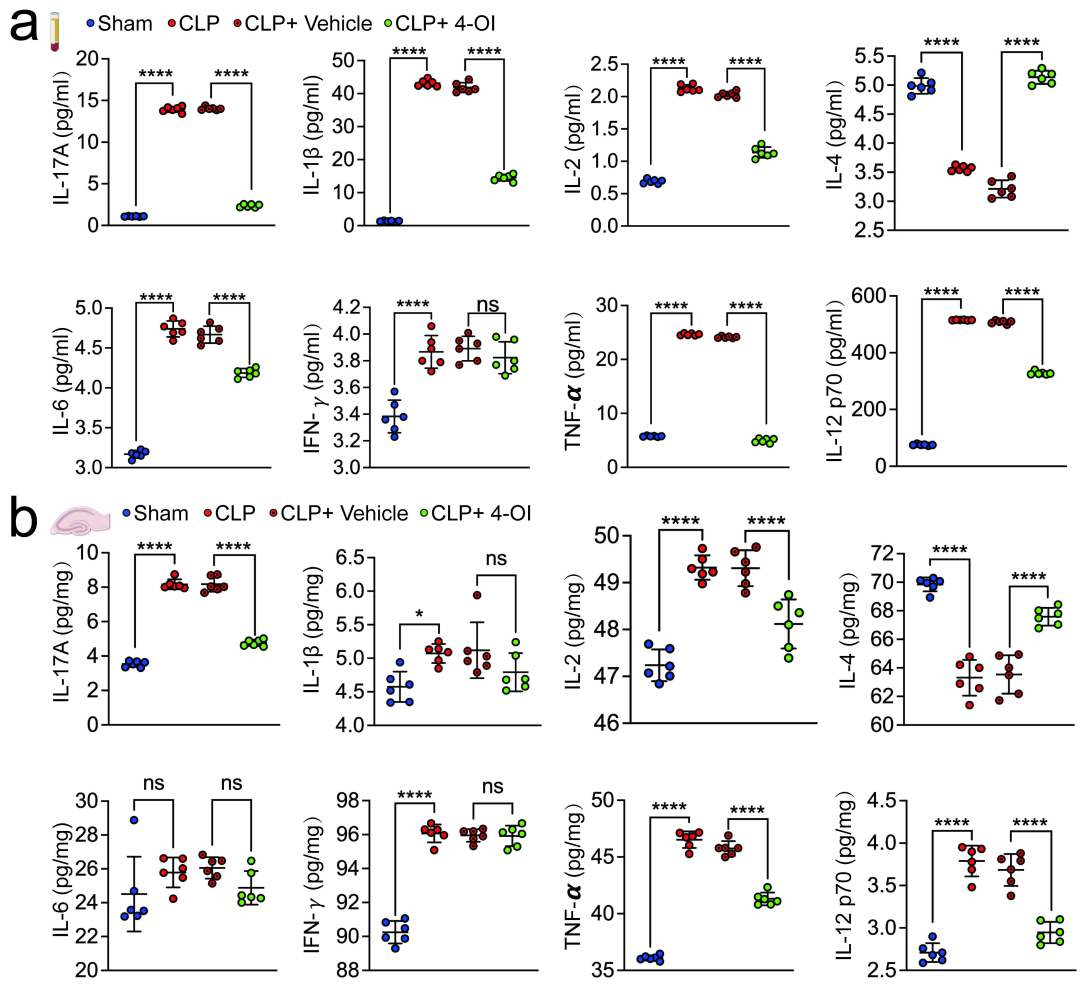

Extended Data Fig. 6. Exogenous 4-OI reduced inflammatory cytokine levels.

a Plasma inflammatory cytokine concentrations in sham-operated and cecum ligation and puncture (CLP) - treated mice administered 4-Octyl itaconate (4-OI) or vehicle (n = 6). **b** Hippocampal inflammatory cytokine concentrations in sham-operated and CLP-treated mice administered 4-OI or vehicle (n = 6). Data are shown as mean ± SD. $^{****}P < 0.0001$. ns, not significant. *P* values were calculated using one-way ANOVA followed by Šídák's multiple comparisons test (a, b).

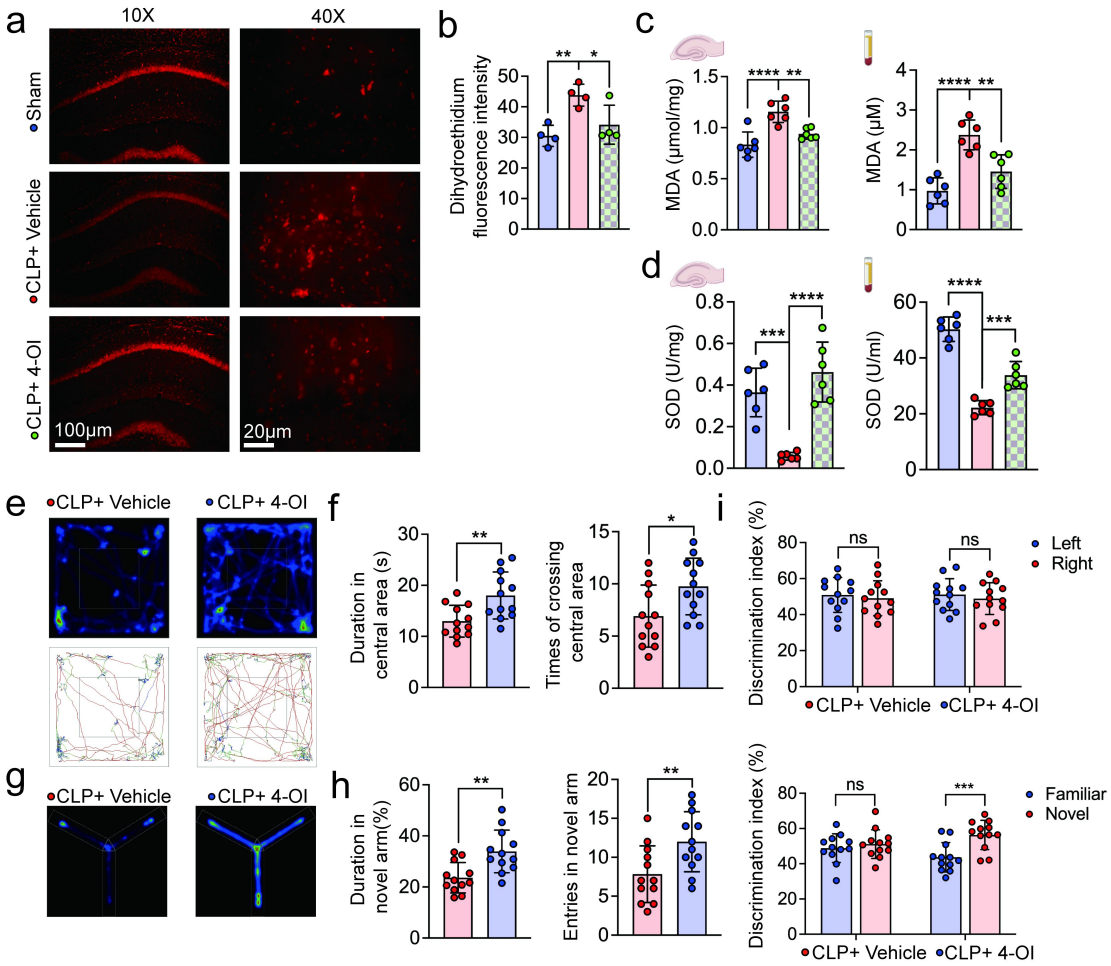

Extended Data Fig. 7. Exogenous 4-OI reduced oxidative stress levels and mitigated SAE.

Representative immunofluorescence images (**a**) and analysis (**b**) of dihydroethidium (DHE) staining in hippocampus (n = 6). **c** Levels of malonaldehyde (MDA) in the hippocampus and plasma of mice (n = 6). **d** Levels of Superoxide dismutase (SOD) in the hippocampus and plasma of mice (n = 6). Representative images (**e**) and statistical analysis (**f**) of open field tests (n = 12). Representative images (**g**) and statistical analysis (**h**) of Y-maze tests (n = 12). **i** Statistical analysis of novel object recognition tests (n = 12). Data are shown as mean ± SD. $^{*}P < 0.05$, $^{**}P < 0.01$, $^{***}P < 0.001$, $^{****}P < 0.0001$. ns, not significant. *P* values were calculated using one-way ANOVA

followed by Šídák's multiple comparisons test (b–d), two-sided Student's unpaired t-tests (f, h) and multiple unpaired t-tests (i).

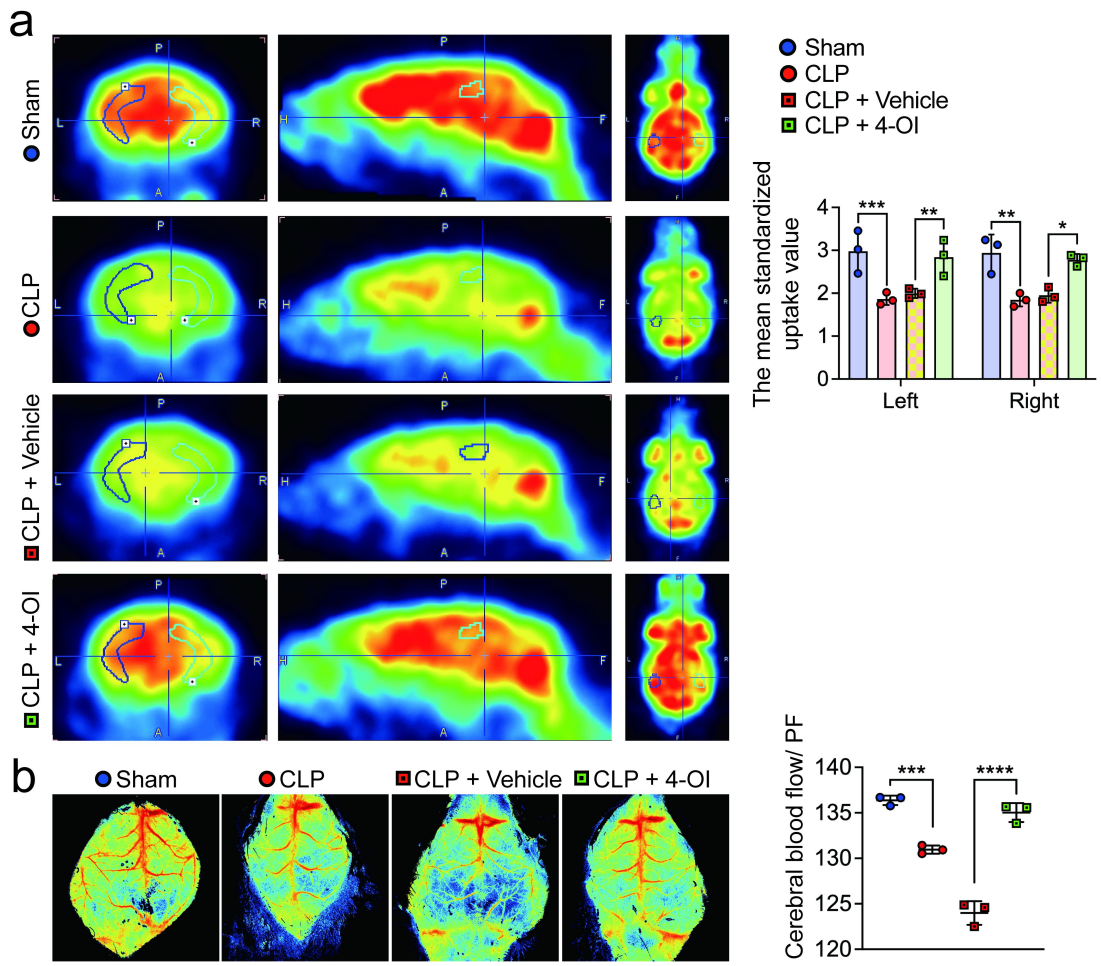

Extended Data Fig. 8. Exogenous 4-Octyl itaconate enhances cerebral metabolism and improves cortical blood flow.

a Representative Positron Emission Tomography (PET) images and analysis of brain glucose metabolism in mice (n = 3). **b** Representative laser speckle imaging and analysis of cortical blood flow in mice (n = 3). Data are shown as mean ± SD. $^{*}P < 0.05$, $^{**}P < 0.01$, $^{***}P < 0.001$, $^{****}P < 0.0001$. *P* values were calculated using two-way ANOVA followed by Šídák's multiple comparisons test (a) and one-way ANOVA followed by Šídák's multiple comparisons test (b).

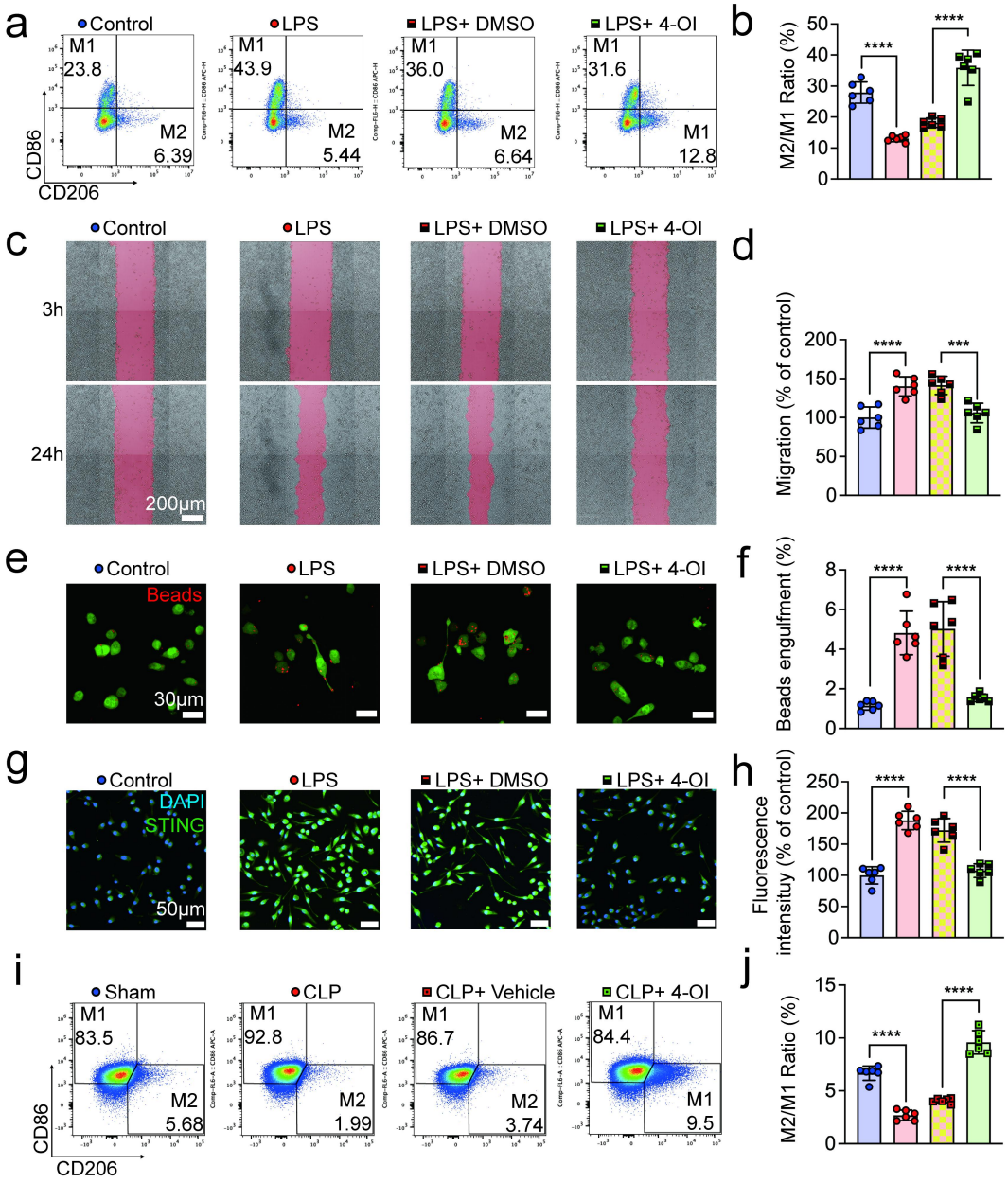

Extended Data Fig. 9. Exogenous 4-OI reduces microglial inflammation and phagocytic capacity.

a, b Representative flow cytometry (FCM) plots showing M1 ($CD86^+$) and M2 ($CD206^+$) phenotypes in BV2 cells following lipopolysaccharide (LPS) and 4-Octyl itaconate (4-OI) treatment. Graph displaying the M2/M1 ratio (n = 6). **c, d** Representative images of scratch assay in BV2 cells treated with LPS and 4-OI. Graph displaying the migration rate (% of control) (n = 6). **e, f** Representative images

of phagocytosis assay in BV2 cells treated with LPS and 4-OI. Graph displaying the beads engulfment (n = 6). **g, h** Representative immunofluorescence images of STING in BV2 cells treated with LPS and 4-OI. Graph displaying the fluorescence intensity (n = 6). **i, j** Representative FCM plots depicting M1 ($CD86^+$) and M2 ($CD206^+$) microglia following CLP and 4-OI treatment. Graph displaying the ratio of M2/M1 (n = 6). Data are shown as mean ± SD. $^{***}P < 0.001$, $^{****}P < 0.0001$. *P* values were calculated using one-way ANOVA followed by Šídák's multiple comparisons test (b, d, f, h, j).

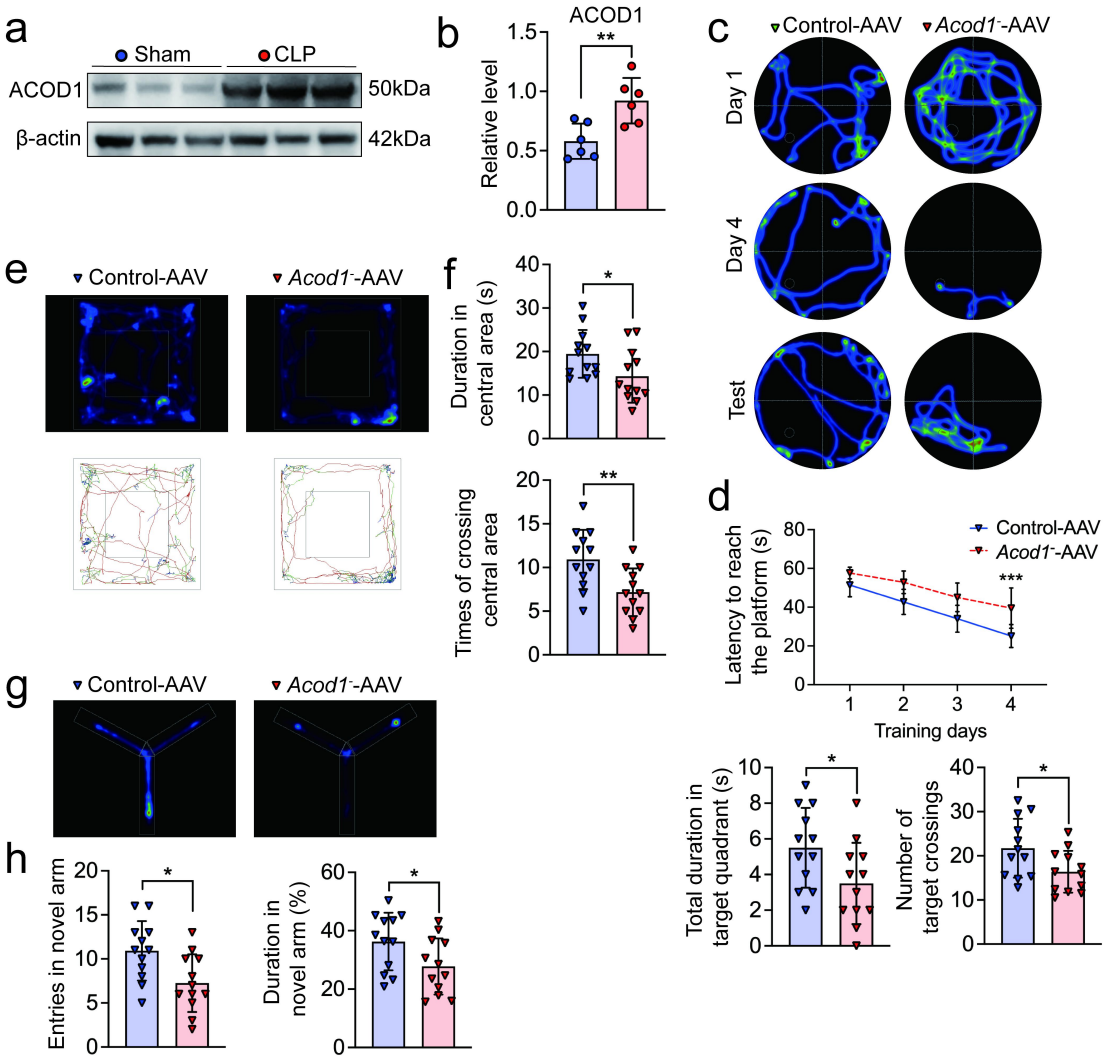

Extended Data Fig. 10. Inhibiting of ACOD1 expression in microglia impaires cognitive function.

Western blot (**a**) and quantification (**b**) of ACOD1 in hippocampus of mice (n = 6). Representative images (**c**) and statistical analysis (**d**) of the Morris water maze (n = 12). Representative images (**e**) and statistical analysis (**f**) of open field tests (n = 12). Representative images (**g**) and statistical analysis (**h**) of Y-maze tests (n = 12). Data are shown as mean ± SD. $^{*}P < 0.05$, $^{**}P < 0.01$, $^{***}P < 0.001$. *P* values were calculated using two-sided Student's unpaired t-tests (b, d, f, h).

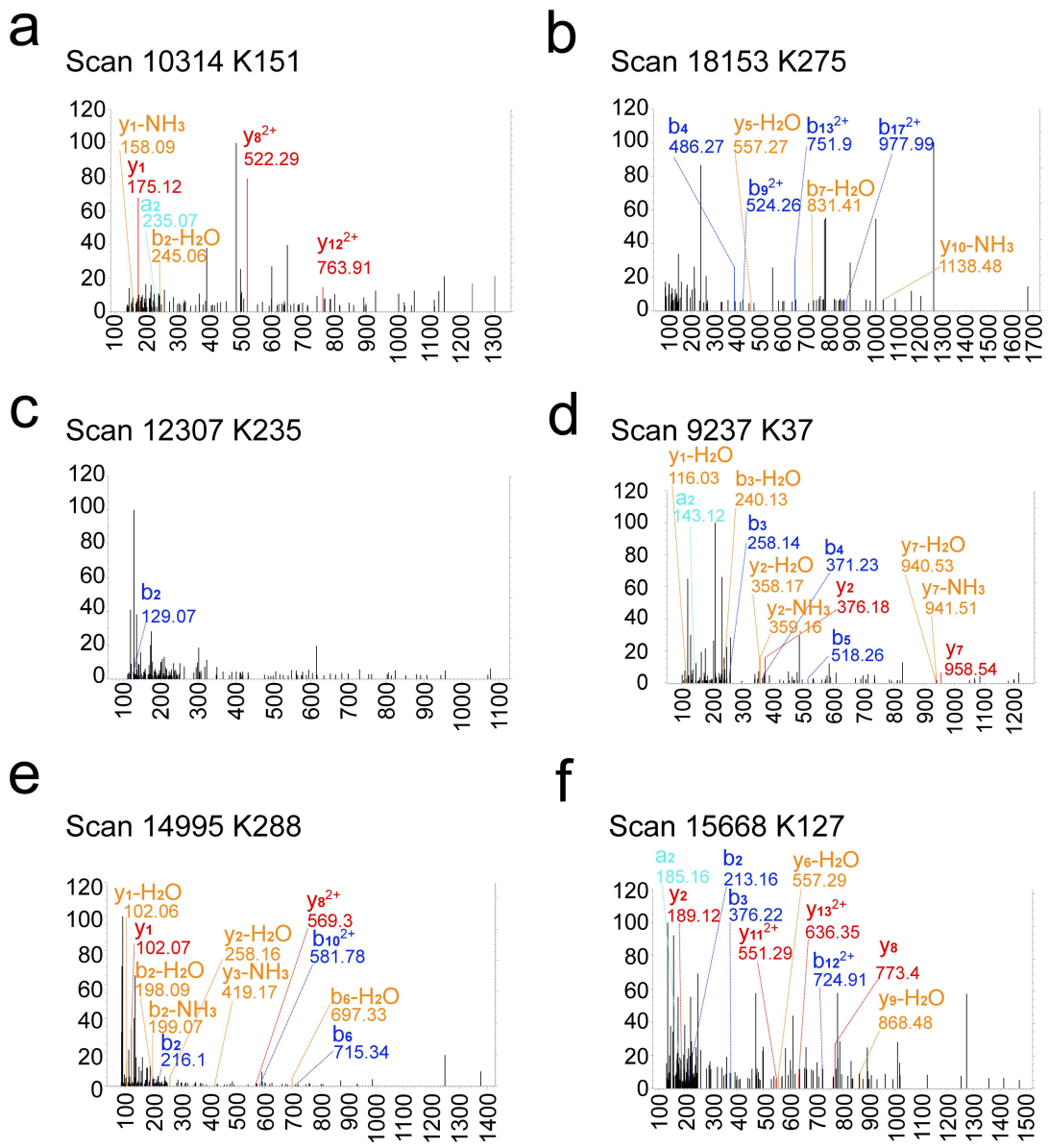

Extended Data Fig. 11. Mass spectrometry identification of STING ubiquitination sites.

Potential ubiquitination sites at lysine 151 (K151) (**a**), lysine 275 (K275) (**b**), lysine 235 (K235) (**c**), lysine 37 (K37) (**d**), lysine 288 (K288) (**e**), and lysine 127 (K127) (**f**) on STING.

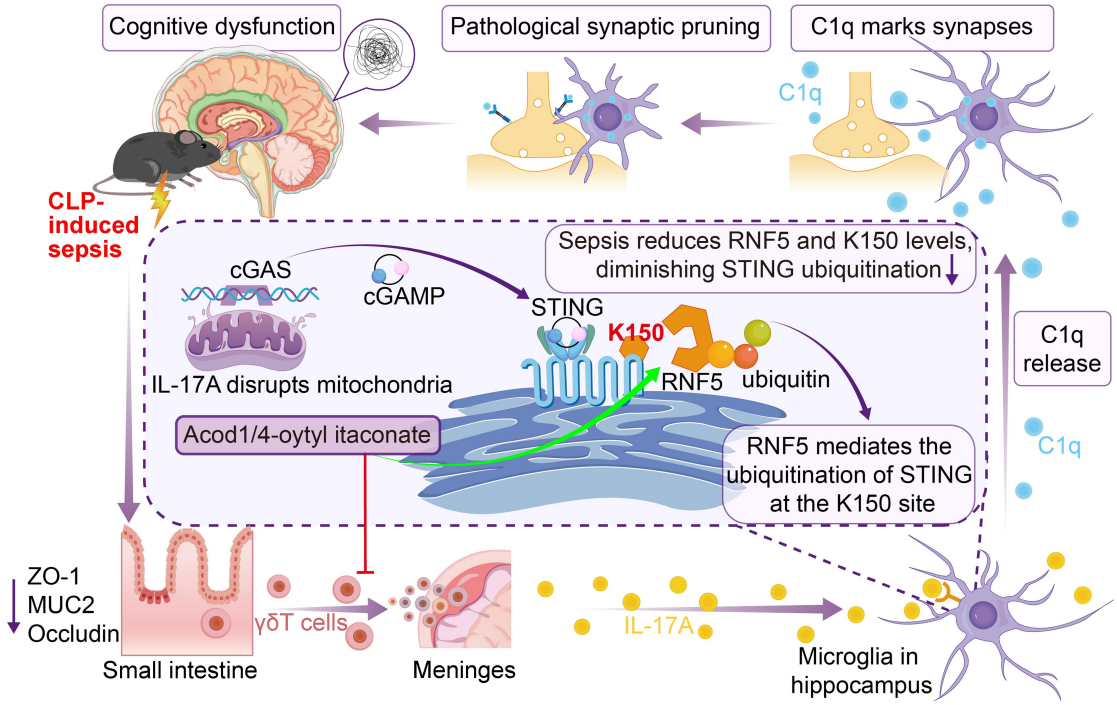

Extended Data Fig. 12. Schematic of mechanism.

During sepsis, IL-7R^{high} CD8^{low} γδ T17 cells migrate from the small intestine to the meninges, where they secrete IL-17A. This secretion activates microglia in the hippocampus, leading to impaired oxidative metabolism and mitochondrial damage. The resulting release of mitochondrial deoxyribonucleic acid (mtDNA) triggers the activation of the cGAS-STING signaling pathway. This activation increases the release of complement component C1q by microglia, enhancing synaptic tagging and causing excessive synaptic pruning. Treatment with 4-Octyl Itaconate (4-OI) has been shown to mitigate sepsis-associated encephalopathy (SAE) by inhibiting the migration of IL-7R^{high} CD8^{low} γδ T17 cells to the meninges following sepsis. Additionally, 4-OI promotes the expression of the ubiquitination site at K150 on STING, facilitating K150-dependent STING ubiquitination, thereby alleviating the effects of SAE.